An Assessment of the Precision and Accuracy of Altimetry Retrievals for a Monterey Bay GNSS-R Experiment

Jake Mashburn[1], Penina Axelrad[1], Stephen Lowe[2], and Kristine M. Larson[1]

[1]Aerospace Engineering Sciences, University of Colorado Boulder, Boulder, CO 80301 USA
[2]Jet Propulsion Laboratory, California Institute of Technology, Pasadena, California

Global Navigation Satellite Systems provide signals of opportunity for bi-static radar remote sensing, called GNSS reflectometry (GNSS-R), that have potential to be used for ocean altimetry. These signals have advantages over traditional mono-static radar that include reduced cost, high density of measurements in time and space, and an inherent reference to a highly accurate time-space frame. Here we examine GNSS-R data collected from an aircraft flying over Monterey Bay, California. A downward-looking dual-frequency left-hand circularly polarized patch antenna recorded reflected signals. An upward-looking commercial antenna recorded the direct signals. Dual frequency carrier phase data from this antenna were also used to produce precise coordinates for the aircraft. The L1 P-code GPS data were collected over four days with two flights per day and consist of nine transects covering a 1 deg $\times 1$ deg grid.

The performance of three timing retrieval algorithms has been evaluated based on measurement precision. From the observed cross-correlation waveform, the specular reflection timing was derived from the delay of the 70% peak correlation power (HALF method), the waveform leading edge peak first derivative (DER method), or the delay associated with a best fit function approximating the nominal waveform shape (PARA3 method). It was found the HALF method produced the most precise measurements for a 5 second integration time with a standard deviation of σ = 0.6 meters.

The measurement accuracy is characterized by comparison with well established models including neutral atmospheric delay, mean sea surface height, and ocean and solid Earth tides. Biases on the order of $1-4$ meters are observed with respect to a modeled mean sea surface and between each flight. However, the measurements are shown to track changes in sea surface height along the ground track to within 0.6 meters.

I. Introduction

THE transmissions from satellites of Global Navigation Satellite Systems (GNSS) represent signals of opportunity for passive bi-static radar remote sensing. The use of these signals and their reflections for remote sensing is commonly called GNSS Reflectometry (GNSS-R). Measurements of sea surface height, sea ice state, and soil moisture fluctuations using these signals have been explored from various static and dynamic platforms [1]–[3]. Specifically for sea surface altimetry, GNSS-R offers several advantages over mono-static radar systems including reduced cost, multiple measurements over a large area, and an inherent reference to a highly accurate time-space frame. Disadvantages relate to the fact that GNSS signals are not optimized for remote sensing applications and thus have limited bandwidth, lower signal power and therefore lower altimetric precision compared to active altimeters.

The application of GNSS-R or sea surface altimetry has been demonstrated from airborne platforms in several campaigns [1], [4]–[8]. The precision of the GNSS-R measurements is heavily dependent on signal to noise ratio, the specular timing retrieval from the reflected waveform, and several other variables. The measurement accuracy is limited by uncalibrated instrument biases and errors in propagation models. To date, a few timing algorithms have been investigated and their precision characterized [4], [6], [9], [10] though altimetric accuracy of code based measurements has not been sufficiently explored. Carrier phase observations have been used in some cases to produce precise and accurate results [4], [7]. Code based measurements have thus far resulted in either imprecise or biased height retrievals [5].

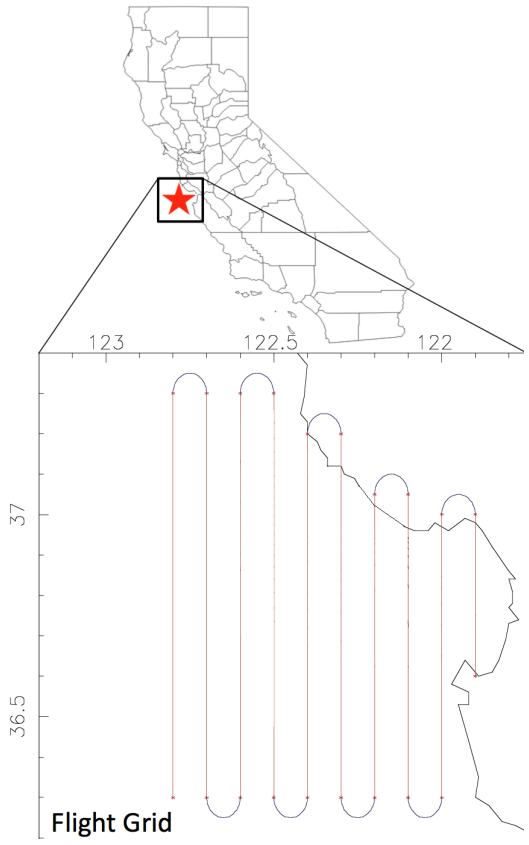

Fig. 1. The planned flight pattern over Monterey Bay, California, USA.

Manuscript received September 15, 2015; revised Janurary 24, 2016.

This paper further investigates these issues based on an airborne experiment conducted in Monterey Bay, California. We first compare the measurement precision of three timing algorithms, similar in aim to Cardellach 2014 [6], to explore the sensitivity of certain points along the correlation waveform and establish a performance baseline for a new method. Then we examine the altimetry measurement accuracy through the implementation of models and altimetric error corrections that rely on scenario geometry, mean and time variant topography, and atmospheric conditions as described by accepted models.

II. Experimental Campaign and Data Set

The following sections provide a description of the 2003 Monterey Bay data collection campaign, the GNSS-R instrument, and an overview of the data set obtained.

A. Data Collection Campaign

In August of 2003 a Cessna 310 was chartered to fly over Monterey Bay along the coast of California. A North-South oriented flight pattern at 0.1 deg longitude intervals was executed as seen in Fig. 1. The pattern extends nearly 1 deg in latitude and longitude and reaches over 60 km from the coastline at its South-West corner. This pattern was flown at a speed of about 90 m/s and an altitude of approximately 3 km. Two flights were conducted each day for several days with one in the morning and a second in the afternoon both lasting about 4 hours. The data examined here were taken from flights completed on the afternoon of August 13 and morning and afternoon of August 15, August 18, and August 19, 2003. The flight on August 13 is denoted as MB4 PM, flights on August 15 as MB5 AM/PM, August 18 as MB6 AM/PM, and August 19 as MB7 AM/PM.

B. GNSS-R Instrument

A conventional GPS receiver and a delay/Doppler mapping receiver designed by JPL were used to perform this experiment [11]. The delay/Doppler mapping receiver included a data recorder on the flight and a separate software defined receiver for post processing. The software receiver employs a clean replica method where a direct signal is tracked and used to drive a replica PRN code that is correlated with the reflected signal. To analyze P(Y) code signals without resorting to codeless or cross-correlating techniques, the replica codes were obtained after the fact and the correlations were done in post processing. The data recorder supports two input channels connected to up-looking and down-looking antennas of right and left handed circular polarization, respectively. These were small patch type antennas with peak gain near 3 dBi. The software receiver was capable of extracting C/A code and P(Y) code waveforms on both L1 and L2 frequencies. For the Monterey Bay experiments the digitally sampled L1 P(Y) signals were correlated and coherently integrated for 10 ms at lags spaced 50 ns apart. A series of 10 ms integrated waveforms were then summed to produce each incoherently integrated waveform as illustrated in Fig. 2. It was with these incoherently integrated waveforms that timing measurements were taken.

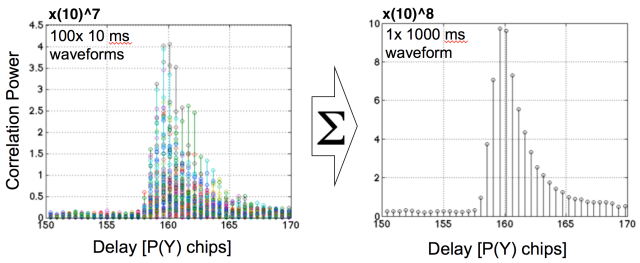

Fig. 2. A one-second incoherently integrated waveform is created by summing one hundred, 10 ms coherently integrated waveforms.

C. Data Set

GPS-R measurements on the L1 frequency and conventional GPS receiver measurements were recorded on board the aircraft platform. At any given time within the data set, as many as four GPS transmitters visible above 45 deg elevation produce strong reflections. Each flight yielded nearly continuous 20 MHz sampling on both I and Q channels producing a large data set. A carrier-phase based point solution was computed for the aircraft position with the NASA JPL GIPSY-OASIS 2 (GOA-2) software. The receiver position solution has an estimated precision of 0.3 meters [Bruce Haines, personal communication, 1/18/2016].

Concurrent data from *in situ* buoys measuring wind speed, atmospheric pressure, temperature, and humidity are available from the NOAA National Data Buoy Center [12] to be used in the delay model described later. Unfortunately, measurements of the aircraft attitude and atmospheric conditions aloft were not recorded during the experiment. Thus, for this analysis the aircraft attitude has been assumed constant when flying straight and level and data from turns are not considered. Atmospheric conditions are taken from the NOAA NCEP Reanalysis data provided by the NOAA/OAR/ESRL PSD, Boulder, Colorado, USA [13].

III. Methodology

The algorithms and models used in this research are now described. First, the tracking methods used to characterize precision are presented, followed by the components of the delay model used to characterize the accuracy.

A. Specular Delay Tracking Algorithms

Several specular timing retrieval algorithms were considered to estimate the time of arrival difference between direct and reflected GPS signals. Each algorithm is applied to a series of waveforms that have been incoherently integrated for $T_{in} = 0.5 - 10$ seconds. The three algorithms are as follows.

1) HALF

The HALF method has been derived from traditional monostatic radar techniques taking the specular reflection delay at a given fraction of the peak correlation power [6], [8]. Here the specular point is assumed to lie at the 70% peak power delay. This point was chosen based on the findings of Cardellach 2014 [6] that showed tracking the 70% point is similar to the theoretically ideal peak derivative point. The HALF delay is

found by using a Newton's method iteration scheme. All three tracking methods model the waveforms with (1) which allows the band limited signals to be interpolated.

$$x(t) = \sum_{n=-\infty}^{\infty} x[n] \cdot sinc\left(\frac{t - nT}{T}\right) \quad (1)$$

Here $x[n]$ represents the series of discrete correlation function samples, t is delay, and T is the sampling period set to be 0.5 P-code chips.

The datum from which the specular timing is measured in the HALF method (and the following algorithms) is the direct signal time of arrival. This "zero" delay is taken to be at the direct signal waveform peak. The true waveform peak is found via interpolation which has the benefit of estimating and removing any DLL tracking errors.

2) DER

The second algorithm, the DER method, derives the specular delay from the maximum first derivative on the waveform leading edge, as would be for the ideal case [14]. The waveform derivative is calculated numerically as a function of delay and the location of the maximum is found by a golden section search method [15]. As with the HALF method, the timing of the direct signal waveform peak is found by a DLL allowing the difference in time of arrival to be computed.

3) PARA3

The third algorithm, a three parameter function fitting method, proposes a new empirical waveform model. The model of the GPS-R waveform is created through the convolution of a simulated squared, band limited auto-correlation function and the function $f(t|\tau, A, \alpha)$ given by (2). The function $f(t|\tau, A, \alpha)$ is a representation of the correlation waveform in the case of infinite bandwidth and chipping rate. The specular reflection takes the shortest possible reflection path to arrive at time τ where the signal return instantaneously rises to amplitude A and decays exponentially in delay with decay rate α. Fig. 3 illustrates the auto-correlation function, $f(t|\tau, A, \alpha)$, and the resultant waveform model.

$$f(t \mid \tau, A, \alpha) = \begin{cases} 0 & t < \tau \\ A \cdot e^{-(t-\tau)/\alpha} & t \geq \tau \end{cases} \quad (2)$$

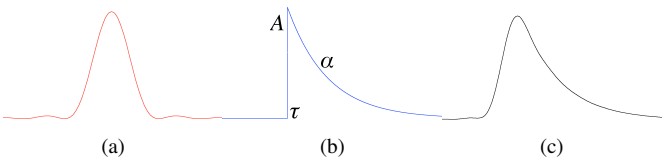

Fig. 3. The (a) band limited auto-correlation function is convolved with (b) a three parameter function $f(t|\tau, A, \alpha)$ to yield the (c) waveform model. The least squares best fit combination τ^*, A^*, and α^* is found and τ^* is taken as the specular reflection time delay.

The parameters τ, A, and α are tuned to achieve a least squares best fit between the model and data. The best fit set of parameters is denoted with a star and τ^* is taken to be the specular delay measurement. The problem of finding the least squares best fit model to the measured waveform is very nonlinear with many local extrema in the parameter state space. A cost function equal to the sum of the squared residuals over the waveform from the peak delay - 2 code chips to the peak + 0.5 code chips is used to evaluate the fit of each model realization. Fitting over this range was found to produce the most precise timing measurements. The global minimum cost is found by first performing a coarse brute force search over a reasonable section of the state space. The coarse best fit solution becomes the initial condition to a steepest descent search that approaches the nearest minimum by following the steepest negative gradient.

It will be seen in Section IV that the PARA3 algorithm did not perform as well as was hoped. Some potential improvements to this method are suggested in Section V.

B. Delay Model

A comprehensive model to predict the path delay of a reflected GPS signal as seen by an airborne receiver has been constructed and used to assess the precision and absolute accuracy of the Monterey Bay GPS-R measurements. Included are a reference surface, ocean tides, solid Earth tides, tropospheric delay, and the zenith-nadir antenna baseline. Missing from this model is the aircraft attitude as that data are not available.

1) Reference Surface

In order to predict the reflected signal path delay, a model of the reflecting surface and the relative receiver-transmitter geometry are taken into account. Here we include the capability to simulate specular reflections from either the WGS84 ellipsoid or the DTU13 mean sea surface [16] with the option to superimpose ocean and solid Earth tide corrections. An iterative approach is used to find the specular reflection location on the surface [17] such that the incident and reflecting angles with respect to the surface normal are equal. The additional path delay of the reflected signal is found by subtracting the line of sight range from receiver to transmitter from the bistatic range.

2) Ocean and Body Tides

Ocean and solid Earth tide corrections may be superimposed onto the reference surface. Tidal corrections have been generated by the GOT4.8 model to cover the extent of the flight path over the experiment times [Richard Ray, personal communication, 2/8/2015]. The model is a summation of short period, long period, load, solid body, and pole tides. A 0.5 deg grid was evaluated at 10 minute intervals throughout the duration of the experiment. At a given location and point in time the modeled tide corrections are interpolated and imposed upon the reference surface. In Monterey Bay the GOT4.8 model estimates the tides to be on the order of ± 1 meter.

3) Tropospheric Path Delay

The excess signal path delay due to the tropospheric effect is accounted for using the modified Saastamoinen model given by (3) with both "wet" and "dry" components [18]. Atmospheric pressure (P), temperature (T), and water vapor pressure (e) are taken from NOAA NCEP Reanalysis data. This modified version of the traditional Saastamoinen model accounts for the receiver altitude through correction terms B and R that depend on height and incidence angle.

$$\delta_T = \frac{0.002277}{sin(\theta)}\left[P + \left(\frac{1255}{T} + 0.05\right)e - B \cdot tan^2(\theta)\right] + R \tag{3}$$

4) Antenna Baseline

In the Monterey Bay experiments, the zenith pointed antenna was mounted on top of the aircraft fuselage while the nadir pointed antenna was mounted beneath the fuselage. Physical measurement of the installation indicated that the nadir pointed antenna was 10 cm left, 10 cm behind, and 125 cm below the zenith antenna in the aircraft body frame (starboard, forward, up). The location of the zenith looking antenna in the WGS84 frame is estimated in the aircraft position solution. The location of the nadir looking antenna in the WGS84 frame was found by transforming the known body frame vector into a local level frame (East-North-Up) with an assumed aircraft attitude and heading and then into the Earth fixed frame. When predicting the specular reflection delay from a model surface the WGS84 frame coordinates of the nadir pointed antenna are used as the receiving point.

Without knowledge of the true aircraft attitude a "straight and level" orientation was assumed (yaw, pitch, and roll are 0 deg). A model to estimate the delay effect of a baseline offset between zenith and nadir antennas is given in (4)

$$\delta_B = (\boldsymbol{R}\,\vec{b}) \cdot \hat{e} \tag{4}$$

where δ_B is the delay effect, $\vec{b}$ is the baseline vector in the body frame, $\boldsymbol{R}$ is the rotation matrix to transform from the body frame to a local level frame via yaw, pitch, roll, and heading angles, and $\hat{e}$ is the receiver-transmitter line of sight unit vector in the local level frame. It can be seen that the delay effect depends on the projection of the baseline vector onto the line of sight direction.

C. Surface Height Retrieval

To retrieve surface height from the bistatic delay measurement the specular delay can be approximately related to the receiver height by (5).

$$\delta^m \approx 2 \cdot h_{RX} \cdot sin(\theta) \tag{5}$$

Here δ^m is the measured specular delay in units of length, h_{RX} is the receiver height, and θ is the GPS elevation angle at the specular point. Since the receiver location is known in the WGS84 frame the reflecting surface can then be positioned in that same frame. However, this model assumes a locally flat Earth and therefore may be in error by several meters at a 3 km receiver altitude. Instead we compute an estimate of the surface height (h^{surf}) relative to a reference surface by comparing measured and predicted path delays. The measured path delay (δ^m) is subtracted from the predicted delay (δ^p_{REF}), computed iteratively as described in Section III-B above, and scaled by twice the sine of the elevation angle (θ) as seen in (6). Using a differential delay between a measurement and prediction brings the problem into the linear regime where the flat Earth approximation may be used. The measured relative surface heights were then assembled into a map to illustrate the measured deviation from the chosen reference. In (6) either the WGS84 ellipsoid or the DTU13 model may be used as the reference.

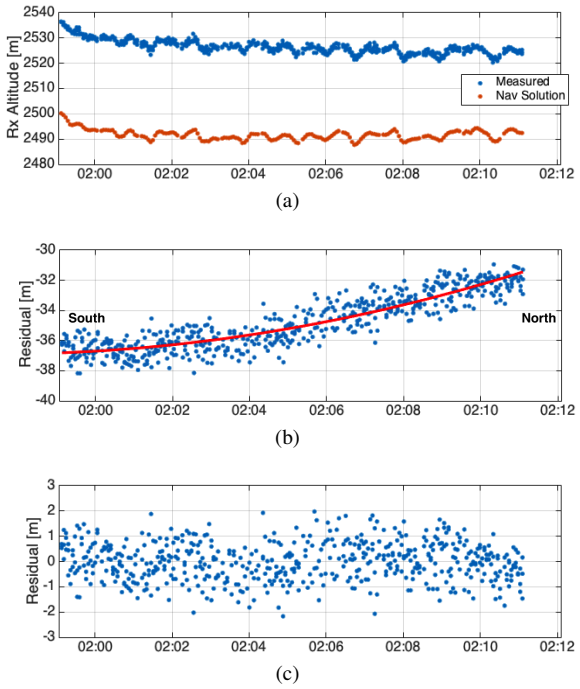

Fig. 4. (a) The measured aircraft heights show a persistent bias away from the WGS84 ellipsoidal heights derived from the aircraft navigation solution. This bias is consistent with the known mean sea surface in Monterey Bay. (b) The measured surface heights relative to the WGS84 ellipsoid show a bias and systematic slope and curvature. (c) Once the first and second order systematic trends are removed, the residuals are zero mean, near white noise.

$$h^{surf} = \frac{\delta^p_{REF} - \delta^m}{2 \cdot sin(\theta)} \tag{6}$$

D. Measurement Precision Calculation

A series of altitude measurements from two passes over Monterey Bay were then used to asses the measurement precision. Measured receiver heights compared to the known aircraft heights above the WGS84 reference ellipsoid are shown in Fig. 4a. Surface heights relative to the WGS84 ellipsoid were retrieved with (6) and are shown in Fig. 4b. In this case the predicted delay was made to account for the WGS84 ellipsoid, troposphere delay, and the antenna baseline effects. The resulting measured surface height has a mean offset and a systematic slope and curvature. The solid red curve represents a least squares quadratic curve fit to emphasize the systematic effects. The quadratic fit was subtracted out to form zero mean, near white noise residuals, Fig. 4c. A quadratic fit rather than a geoid model was used to avoid the influence of any model errors. The standard deviation of the residuals is computed and reported as the measurement precision. Average standard deviation values over two legs of the flight furthest from shore with three visible transmitters each and for several incoherent integration times are reported in Table I. The precision was computed for each delay tracking algorithm. The best performing algorithm was used to then characterize accuracy.

IV. Results

A. Precision

The metric by which performance of each timing algorithm has been graded is the standard deviation of the altitude measurement residuals. Table I shows the standard deviation of the residuals for each algorithm for various incoherent integration times. It can be seen that the HALF algorithm outperforms both PARA3 and DER in all cases. The PARA3 algorithm performs second best for integration times 0.5 sec, 1 sec, and 2 sec. This result indicates that the HALF algorithm is the most precise.

The HALF method outperforming DER is an expected result. First, the DER method is tied to a noisy measurement point. The correlation waveform samples have noise on them and therefore the derivative, which is being computed numerically, is expected to have even more noise. Second, the DER method tracks a rounded peak which is difficult to find precisely with numerical methods. In contrast, HALF tracks a zero crossing which is a more precise, well defined point.

It can be seen in Table I that the PARA3 algorithm does not perform as well as the other methods as the integration time is increased. The standard deviations from the HALF and DER methods decrease by a factor of $\sqrt{T_{in}}$ as the integration time is increased. The PARA3 standard deviations do not. For example, there is a factor of four increase in integration time from 0.5 sec to 2 sec. It is expected that the standard deviation of the measurement residual would be reduced by a factor of two as the incoherent noise is averaged down. For the HALF and DER algorithms this is the case (HALF $\sigma_{0.5s}/\sigma_{2s} = 1.9$ and DER $\sigma_{0.5s}/\sigma_{2s} = 2.0$) but the PARA3 σ values only reduce by a factor of 1.5.

TABLE I
STANDARD DEVIATION OF ALTITUDE MEASUREMENT RESIDUALS FOR EACH OF THE THREE TIMING ALGORITHMS OVER VARIOUS INCOHERENT INTEGRATION TIMES.

T_{in}[s]	HALF σ [m]	PARA3 σ [m]	DER σ [m]
0.5	1.7	1.8	2.8
1	1.2	1.4	2.0
2	0.9	1.2	1.3
5	0.6	1.0	0.9
10	0.5	0.9	0.7

A chi squared (χ^2) test for goodness of fit has been performed to analyze the quality of the PARA3 waveform model fit. As an example the χ^2 per degree of freedom was calculated for each waveform in a set of 5 sec incoherently integrated waveforms (17 waveforms). If the model were in good agreement with the measured data, the χ^2 value would be near a value of 1, $\chi^2 \approx 1$. In this case the χ^2 values range from 15 to 55 with a mean of $\chi^2 = 34$ indicating poor agreement between the model and data.

Use of the direct signal correlation waveform instead of a simulated auto-correlation function may improve fitting in future work. It may be that there are scattering effects that are not being taken into account with this model. In the presence of ocean waves with sufficient height the instantaneous rise in the function $f(t|\tau, A, \alpha)$ would more correctly have some finite slope as reflections from a wave crest arrive at the receiver earlier than those from a wave trough. Perhaps also the exponential decay of $f(t|\tau, A, \alpha)$ with rate α is not representative of the true scattering fall off.

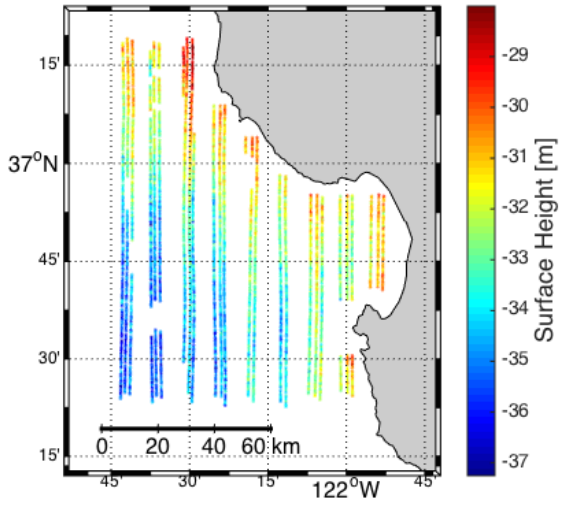

Fig. 5. Individual measurements of Monterey Bay surface as derived from 5s incoherently integrated waveforms recorded during the afternoon flight of August 13, 2003. Each height measurement has been corrected for tropospheric delays, tides, aircraft motion, and the antenna baseline.

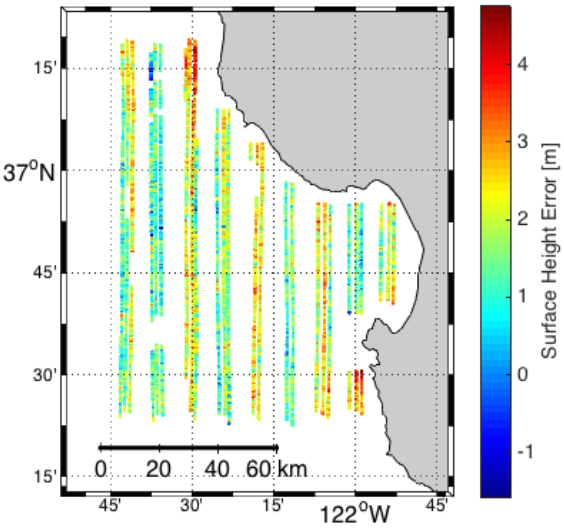

Fig. 6. The difference between each 5s integrated surface height measurement (Fig. 5) and the DTU13 mean sea surface model.

B. Accuracy

In the assessment of the measurement accuracy, 5 sec incoherently averaged waveforms and the HALF timing algorithm were used. Corrected measured surface heights were compared against both the WGS84 ellipsoid and the DTU13 mean sea surface. Fig. 5 shows each measured surface height with respect to the WGS84 ellipsoid as retrieved from a 5 sec waveform observed during the afternoon flight of August 13, 2003, MB4 PM. Here the surface height measurements have been corrected for tropospheric delays, tides, aircraft motion,

and the antenna baseline as described above. It can be seen that the surface is approximately 30 m below the ellipsoid and is sloping down into the South and West. From North to South the surface appears sloped downward by about 7 meters over 100 km (0.9 degrees latitude).

The measurements were also compared to the modeled delays predicted using the DTU13 mean sea surface. Fig. 6 illustrates this deviation between the measurements and the mean sea surface model. A positive error indicates that the measured surface is above the reference. It can be seen that there is a meter level positive bias. A similar bias is seen in the other flights as well. This bias is most likely the result of an uncalibrated instrument and the somewhat arbitrary tracking point used in the HALF timing algorithm. Aside from the over all bias, the estimates along the Northern and South-Eastern borders show the largest deviation from the DTU 13 reference surface. While these measurements are taken relatively close to land, they are limited to 2 km offshore to prevent contamination from land reflections. In these coastal areas the mean sea surface and tidal models are known to be less accurate, but not at the level of the observed discrepancy. The mean sea surface and ocean tide models are quoted to be accurate at the 10 cm level in coastal regions [19].

Looking closely at Fig. 6 a striped pattern that is oriented North-South along the flight transects can be observed. Alternating transects appear more red/yellow while those in between appear more blue/green. This pattern can be seen more clearly when the same data are plotted against time in Fig. 7. It can be seen that with respect to the DTU13 mean sea surface the measurements appear to oscillate up and down about a mean bias from one flight leg to the next. Measurements from all visible satellites follow the same pattern as the colored clouds of data corresponding to specific PRNs move together. It appears that this effect may be a function of the aircraft direction of travel (ie. North-bound or South-bound). Or there may be some dependence on transmitter azimuth with respect to the aircraft body frame.

We considered the possibility that the level shift from one direction to the other could be due to an error related to the satellite azimuth, for example an antenna effect. It is known that the nadir pointed antenna gain pattern is skewed to the starbord direction resulting in stronger signal returns from starbord reflections. However, the fact that all of the measurements regardless of their azimuth exhibit similar behavior in Fig. 7 indicates that the measurement is insensitive to antenna gain differences.

Timing errors between the receiver location and delay measurements could also produce an effect similar to what is observed. We investigated this as well, and found that introducing a range of potential timing offsets significantly degraded the results by misaligning the actual aircraft height variations used in computing the predicted ranges from the corresponding measurements. Therefore, if a timing error were present the receiver motion would not be canceled correctly and even larger systematic trends would be present.

The influence of aircraft attitude rotating the antenna baseline would give an effect that is dependent on the direction of travel but the baseline vector in this experiment is simply too small to produce the observed discrepancies between legs. If a reasonable 5 deg angle of attack is assumed, the delay effect associated with the baseline vector in a 180 deg turn is only 0.25 meters for a 55 deg GPS elevation angle. Mapped to height the effect becomes 0.15 meters, much smaller than the observed meter level jumps.

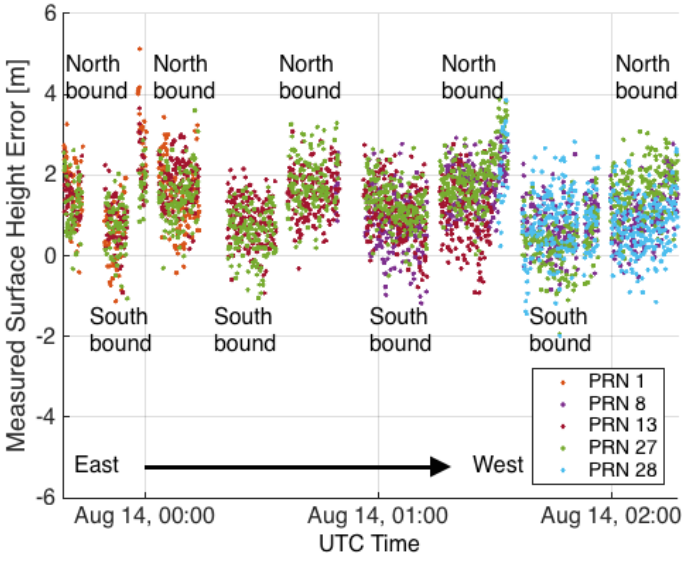

Fig. 7. The difference between the measured surface retrieval and the DTU13 mean sea surface corrected for ocean and body tides plotted against time during the afternoon flight on August 13, 2003.

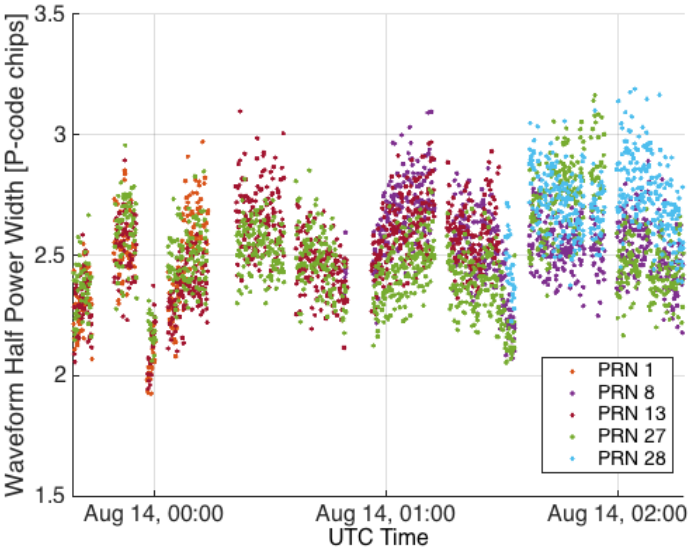

Fig. 8. Correlation waveform width measured at the 50% power point shown as a function of time during the afternoon flight on August 13, 2003, MB4 PM.

The sea surface oscillations that our retrievals seem to show are not consistent with accepted models of this region, and we can only assume at this point that they reflect remaining discrepancies. The model surface shows a relatively smooth, steady negative slope from North-East to South-West. In contrast the measured surface shows a rippled pattern oriented North to South on the surface. We speculate that these biases

may be due in part to phase windup in the aircraft position solution, or there may be some aircraft speed dependence. It has been found that the aircraft persistently flew $10-15$ m/s faster when traveling North-bound.

Another effect that can be seen in Fig. 7 is a slope in the height error as a function of latitude. In several flight transects the height error appears to be lower at the South than at the North. It has been found via *in situ* buoy measurements that the wind speed is different by several meters per second at the North and South ends of the flight grid [12]. It is believed this has caused a difference in surface roughness from North to South and therefore a difference in the signal scattering. Rougher waters will yield more diffuse reflections and therefore alter the shape of the correlation waveform.

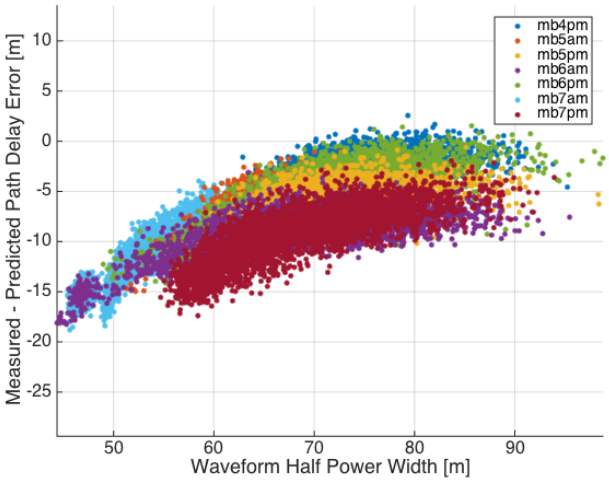

Fig. 9. Measured - predicted delay error against correlation waveform width measured at the 50% power point. The dependence on waveform width illustrates the need for a roughness dependent delay tracking method.

One can use the width of each correlation waveform at the 50% power point as a metric to see the roughness effect on waveform shape. Fig. 8 shows that the correlation waveforms are wider in the South and more narrow in the North as expected. As the wind is stronger in the South there is a rougher surface and therefore a more diffuse reflection and wider waveform. The HALF timing algorithm appears to be sensitive to this change in waveform shape resutling in a timing bias. A roughness dependent timing error would produce the sloped effect seen in the height errors of Fig. 7.

Fig. 9 shows measured - predicted path delay error against waveform half power width for all of the flights studied here. There is an obvious dependence on width (believed to be a proxy for roughness) in the delay error. A remaining bias between flights prevents development of a width dependent empirical delay correction. For example flight MB7 PM is biased with respect to flight MB6 PM by about -5 meters. The source of this inter-flight bias remains unknown. If the measured reflection is purely specular the observed waveform should be an attenuated and delayed version of the direct signal waveform, rather than a spread signal. The correct tracking point would be the waveform peak. For the given receiver bandwidth of this data set the mean delay offset between the

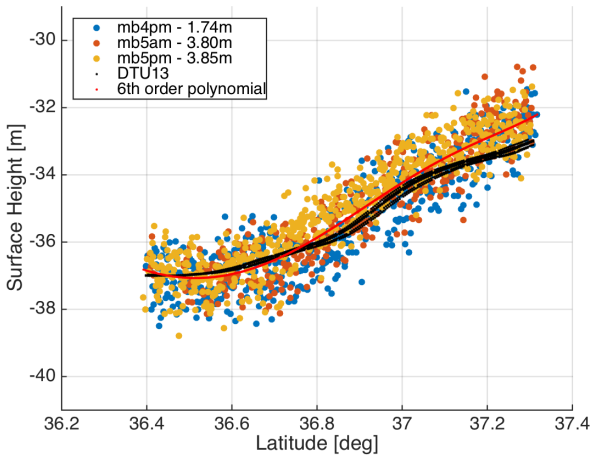

(a)

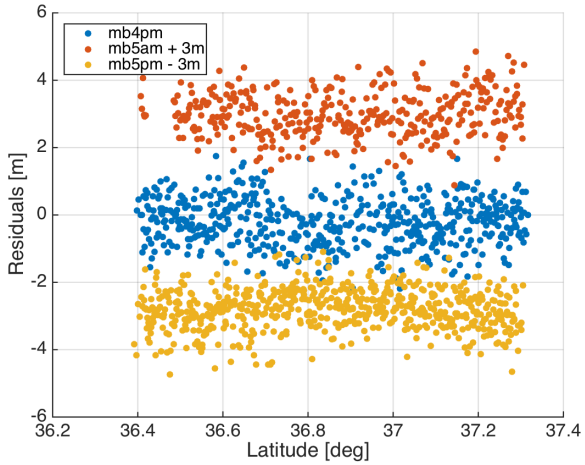

(b)

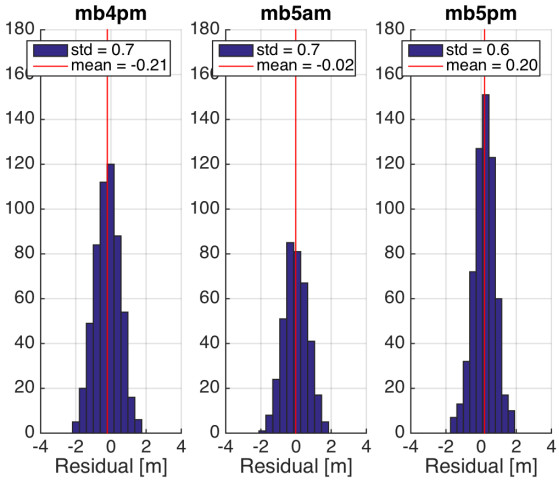

(c)

Fig. 10. (a) The measured surface heights from all four flights over leg #9 biased to have zero mean residuals from the DTU13 mean sea surface (black). A 6th order polynomial is fit to the data from all four flights and shown in red. The residuals of each flight over leg #9 from a 6th order polynomial fit shown against (b) latitude and (c) in histograms.

HALF 70% tracking point and the waveform peak is about 15 meters as measured from the direct signal waveforms. In Fig. 9 as the waveform width narrows, approaching a purely specular reflection, the delay error of the HALF tracking point approaches -15 meters. When the measured reflection has a strong diffuse component the true tracking point moves down the waveform leading edge approaching the maximum derivative tracking point (or similarly the HALF point). Fig. 9 illustrates this behavior as the waveform width is widened from 50 meters (largely specular) to 90 meters (largely diffuse) and the delay error approaches zero.

Results shown thus far in Fig. 5 - 8 are from the flight conducted on the afternoon of August 13, 2003, MB4 PM. The other flights can be described by the same patterns though there is a different meter level bias in the measured surface height between each of them that is attributed to instrument error and the HALF method measurement bias. Aside from the inter-flight biases, the structure of each measurement set is consistent. The North-bound to South-bound discrepancies are present and repeated in all flights and the topography measured along each flight leg is repeated between flights. For example three passes along the Westernmost leg (leg #9) can be compared from flights MB4 PM, MB5 AM, and MB5 PM. After applying all corrections, the measurements of each flight are biased from the DTU13 mean sea surface by $1-4$ meters. Each flight has been shifted to align with the DTU13 model such that they have zero mean residuals. Doing this illustrates the measurement repeatability as seen in Fig. 10a. Each flight has measured the same surface topography, the mean sea surface. To quantify the consistency in shape a single polynomial was fit to all three repeats of leg #9.

Each flight was compared to that polynomial individually. Plotted against latitude the residuals with respect to the polynomial appear flat, near zero mean, and near white noise, Fig. 10b. Histograms shown in Fig. 10c illustrate the residual distribution which looks nearly Gaussian. A chi-squared test for goodness of fit reveals that the polynomial fit to all three passes at once is an excellent representation of each repeat individually and therefore quantitatively shows each flight yields a consistent form. The chi-squared per degree of freedom value is $\chi^2 = 0.99$ for all flights over leg #9. Some systematic errors on the order of 0.5 m with respect to the DTU13 mean sea surface remain.

V. Conclusions and Future Work

Out of the three timing retrieval methods investigated here it has been shown that the HALF algorithm yields the most precise results. However, there is one drawback in that the method tracks an arbitrary point on the correlation waveform. In this case 70% of the peak power was chosen. Tracking the 60% power point would be equally justifiable. Such an arbitrary point leads to measurement biases that in the future will need to calibrated.

The PARA3 method did not meet expectations and the implementation stands to be improved. However, whether this method has the potential to match or surpass HALF is unknown. In future work the following improvements should be considered for the PARA3 method.

1) Use a measured direct signal waveform in place of the simulated auto-correlation function when constructing the PARA3 waveform model.
2) Add a 4^{th} parameter to the function $f(t|\tau, A, \alpha)$ that will describe a finite leading edge slope from zero to amplitude A.
3) Explore a non-exponential decay of the function $f(t|\tau, A, \alpha)$.

There are some improvements and future work to be done in regards to the measurement accuracy assessment as well. There are mean biases, and systematic trends in the height measurement error with respect to the DTU13 mean sea surface that have been left uncorrected. The following steps should be taken.

1) Include a full scattering model to simulate waveforms and track delays.
2) Develop a roughness (or waveform width) dependent "simple" tracking algorithm.
3) Incorporate localized mean surface and tidal models.

Despite some systematic errors, a simple bias correction shows that this data set is consistent and repeatable. After applying corrections for tides, tropospheric delays, aircraft motion and the antenna baseline the repeated measurements of the surface are repeatable and consistent with the others. This result gives confidence that the time and geometry dependent corrections are valid and have been applied correctly.

A foundation for GNSS-R altimetry has been built here that can be adapted to the spaceborne case. These models and altimetry corrections will be adapted and used with publicly released data from TechDemoSat-1 of Surrey Satellite Technologies. Beyond adapting these existing models, models for ionospheric delays and adjustments for spacecraft motion will need to be implemented.

Acknowledgment

This research was supported by the National Aeronautics and Space Administration Jet Propulsion Laboratory. The authors would like to thank Victor Zlotnicki, Richard Ray, Bruce Haines, and Dallas Masters for their valuable contributions.

References

[1] S. Lowe, C. Zuffada, J. LaBrecque, M. Lough, J. Lerma, and L. Young, "An ocean-altimetry measurement using reflected GPS signals observed from a low-altitude aircraft," in *Geoscience and Remote Sensing Symposium, 2000. Proceedings. IGARSS 2000. IEEE 2000 International*, vol. 5, 2000, pp. 2185–2187 vol.5.

[2] F. Fabra, E. Cardellach, A. Rius, S. Ribo, S. Oliveras, O. Nogues-Correig, M. Rivas, M. Semmling, and S. D'Addio, "Phase altimetry with dual polarization GNSS-r over sea ice," *Geoscience and Remote Sensing, IEEE Transactions on*, vol. 50, no. 6, pp. 2112–2121, June 2012.

[3] K. M. Larson, E. E. Small, E. D. Gutmann, A. L. Bilich, J. J. Braun, and V. U. Zavorotny, "Use of GPS receivers as a soil moisture network for water cycle studies," *Geophysical Research Letters*, vol. 35, no. 24, pp. n/a–n/a, 2008, l24405.

[4] A. M. Semmling, J. Wickert, S. Schn, R. Stosius, M. Markgraf, T. Gerber, M. Ge, and G. Beyerle, "A zeppelin experiment to study airborne altimetry using specular global navigation satellite system reflections," *Radio Science*, vol. 48, no. 4, pp. 427–440, 2013.

[5] H. Carreno-Luengo, H. Park, A. Camps, F. Fabra, and A. Rius, "GNSS-r derived centimetric sea topography: An airborne experiment demonstration," *Selected Topics in Applied Earth Observations and Remote Sensing, IEEE Journal of*, vol. 6, no. 3, pp. 1468–1478, June 2013.

[6] E. Cardellach, A. Rius, M. Martin-Neira, F. Fabra, O. Nogues-Correig, S. Ribo, J. Kainulainen, A. Camps, and S. D'Addio, "Consolidating the Precision of Interferometric GNSS-R Ocean Altimetry Using Airborne Experimental Data," *Geoscience and Remote Sensing, IEEE Transactions on*, vol. 52, no. 8, pp. 4992–5004, 2014.
[7] M. Semmling, G. Beyerle, J. Beckheinrich, M. Ge, and J. Wickert, "Airborne GNSS reflectometry using crossover reference points for carrier phase altimetry," in *Geoscience and Remote Sensing Symposium (IGARSS), 2014 IEEE International*, July 2014, pp. 3786–3789.
[8] D. Masters, P. Axelrad, V. Zavorotny, S. Katzberg, and F. Lalezari, "A passive GPS bistatic radar altimeter for aircraft navigation," in *Proceedings of the 14th International Technical Meeting of the Satellite Division of The Institute of Navigation (ION GPS 2001)*, September 2001, pp. 2435–2445.
[9] S. T. Lowe, C. Zuffada, Y. Chao, P. Kroger, and L. E. Young, "5-cm Precision aircraft ocean altimetry using GPS reflections," *Geophysical Research Letters*, vol. 29, no. 10, May 2002.
[10] S. D'Addio, M. Martin-Neira, and C. Buck, "End-to-end performance analysis of a paris in-orbit demostrator ocean altimeter," in *Geoscience and Remote Sensing Symposium (IGARSS), 2011 IEEE International*, July 2011, pp. 4387–4390.
[11] S. Lowe, P. Kroger, G. Franklin, J. LaBrecque, J. Lerma, M. Lough, M. Marcin, R. Muellerschoen, D. Spitzmesser, and L. Young, "A delay/doppler-mapping receiver system for GPS-reflection remote sensing," *Geoscience and Remote Sensing, IEEE Transactions on*, vol. 40, no. 5, pp. 1150–1163, May 2002.
[12] NOAA. (2015, Sept. 15) National data buoy center. [Online]. Available: http://www.ndbc.noaa.gov/
[13] F. Mesinger, G. DiMego, E. Kalnay, K. Mitchell, P. C. Shafran, W. Ebisuzaki, D. Jović, J. Woollen, E. Rogers, E. H. Berbery, M. B. Ek, Y. Fan, R. Grumbine, W. Higgins, H. Li, Y. Lin, G. Manikin, D. Parrish, and W. Shi, "North american regional reanalysis," *Bulletin of the American Meteorological Society*, vol. 87, no. 3, pp. 343–360, 2015/09/14 2006. [Online]. Available: http://dx.doi.org/10.1175/BAMS-87-3-343
[14] G. A. Hajj and C. Zuffada, "Theoretical description of a bistatic system for ocean altimetry using the GPS signal," *Radio Science*, vol. 38, no. 5, 2003.
[15] M. T. Heath, *Scientific Computing: An Introductory Survey*, 2nd ed., E. M. Munson, Ed. McGraw-Hill Higher Education, 1996.
[16] O. Andersen, P. Knudsen, and L. Stenseng, "The DTU13 MSS (mean sea surface) and MDT (mean dynamic topography) from 20 years of satellite altimetry," in *International Association of Geodesy Symposia*, 2015.
[17] S.-C. Wu, T. Meehan, and L. Young, "Potential use of GPS signals as ocean altimetry observables," in *Proceedings of the National Technical Meeting, Institute of Navigation*, Santa Monica, CA, USA, 1997, pp. 543 – 550.
[18] B. Hofmann Wellenhof, H. Lichtenegger, and J. Collins, *Global Positioning System: Theory and Practice*. Springer-Verlag Wien, 1997.
[19] D. Stammer, R. D. Ray, O. B. Andersen, B. K. Arbic, W. Bosch, L. Carrre, Y. Cheng, D. S. Chinn, B. D. Dushaw, G. D. Egbert, S. Y. Erofeeva, H. S. Fok, J. A. M. Green, S. Griffiths, M. A. King, V. Lapin, F. G. Lemoine, S. B. Luthcke, F. Lyard, J. Morison, M. Mller, L. Padman, J. G. Richman, J. F. Shriver, C. K. Shum, E. Taguchi, and Y. Yi, "Accuracy assessment of global barotropic ocean tide models," *Reviews of Geophysics*, vol. 52, no. 3, pp. 243–282, 2014.

Jake Mashburn is a Ph.D. student in the Department of Aerospace Engineering Sciences at the University of Colorado.

Penina Axelrad is Professor and Chair of Aerospace Engineering Sciences at the University of Colorado Boulder. She has been involved in GPS related research since 1986. Dr. Axelrad is a Fellow of the ION and the AIAA, a former president of the IION, and a member of the National Space-Based PNT Advisory Board.

Kristine Larson is a Professor of Aerospace Engineering Sciences at the University of Colorado. Her current research focuses on GPS reflections.

Stephen Lowe Stephen T. Lowe received a B.S. degrees in physics and in mathematics from the Colorado School of Mines, Golden, CO, USA, and a Ph.D. degree in high-energy particle physics from the Stanford University, Stanford, CA, USA. Since 1987, he worked with the Tracking Systems and Applications group, Jet Propulsion Laboratory, California Institute of Technology, Pasadena, CA, USA.